Journal of Applied Polymer Science

Ultraporous Poly(lactic acid) Scaffolds with Improved Mechanical Performance Using High-Pressure Molding and Salt Leaching

Jin Zhang,[1] Ding-Xiang Yan,[1] Jun Lei,[1] Jia-Zhuang Xu,[1] Benjamin S. Hsiao,[2] Zhong-Ming Li[1]

[1]College of Polymer Science and Engineering, State Key Laboratory of Polymer Materials Engineering, Sichuan University, Chengdu, Sichuan 610065, People's Republic of China

[2]Department of Chemistry, Stony Brook University, Stony Brook, New York 11794-3400

Correspondence to: Z. Li (E-mail: zmli@scu.edu.cn)

ABSTRACT: A novel processing technique, i.e. high-pressure compression molding/salt leaching, was developed to fabricate ultraporous poly(lactic acid) (PLA) scaffolds. The optimized composition was studied in relation to the porosity, pore morphology, thermal property, and mechanical performance of the PLA scaffolds. At a porogen ($CaCO_3$) content of 90 wt %, the scaffolds have an interconnected open pore structure and a porosity above 80%. It was truly interesting that the structural stability of high-pressure molded scaffolds was remarkably improved based on the fact that its glass transition temperature (83.5°C) increased about 20°C, as compared to that of the conventional compression-molded PLA (60°C), which is not far from physiological temperature (~37°C) at the risk of structural relaxation or physical aging. More importantly, the mechanical performance of PLA scaffolds was drastically enhanced under optimized processing conditions. At pressure and temperature of 1000 MPa and 190°C, the porous PLA scaffolds attained a storage modulus of 283.7 MPa, comparable to the high-end value of trabecular bone (250 MPa) ever reported. In addition, our prepared PLA scaffolds showed excellent cellular compatibility and biocompatibility *in vitro* tests, further suggesting that the high-pressure molded PLA scaffolds have high potential for bone tissue engineering applications. © 2013 Wiley Periodicals, Inc. J. Appl. Polym. Sci. 130: 3509–3520, 2013

KEYWORDS: bioengineering; biopolymers and renewable polymers; porous materials; structure-property relations; polyesters

Received 22 April 2013; accepted 22 May 2013; Published online 25 June 2013
DOI: 10.1002/app.39570

INTRODUCTION

Nowadays, growing interest is given to the exploitation of porous scaffolds, the biodegradable substrate for cell adhesion and tissue regeneration. In comparison with traditional surgical treatment, such as implantation of a healthy organ from donor, porous scaffolds can effectively overcome the problems of immune rejection from the patient as well as the lack of available donors. Additionally, they provide enough space for cell proliferation and play an important role in transforming the cultured cells to a new tissue.[1] An ideal engineering scaffold is designed to be colonized by cells, whose viability will depend on the porosity and the mechanical and chemical stimuli it receives within.[2–4] Therefore, it is recognized that the scaffolds should be three-dimensional, highly porous, biocompatible, easy to manufacture, and with appropriate mechanical properties.[5,6] Numerous biodegradable synthetic polymers have been widely utilized as scaffolds in the past decade, such as poly(α-hydroxy esters), poly(ethylene glycol), poly(ε-caprolactone), and poly(orthoesters).[7] Among them, poly(lactic acid) (PLA) is the most attractive candidates for scaffold materials. *In vitro* experiments done by Mikos and Temenoff,[8] they discovered that PLA scaffolds had the highest survival rate of cells as compared with other aforementioned polymers, which was mainly related with its favorable mechanical properties, processability, and biocompatibility.

Most studies focus on optimization of PLA scaffolds design from a biochemical point of view, just like biocompatibility or cell adhesion-promoting surfaces,[9,10] but ignored the severe challenge they faced today: polymeric foams may not have the capacity to withstand higher loads without compromising porosity. It is well known that the structure of scaffolds should be with high pore interconnectivity to allow the internal flow required to cell colonization, transport of nutriments, and waste products through the material.[11,12] However, with the increase of pores number and size, the stiffness of scaffolds might be destroyed. As Chandrasekhar[7] once reported, when the porosity of PLA scaffolds increased to 92%, their storage modulus is only 4.72 MPa, which seriously hinders their application in

load-bearing fields. The concept of composite scaffolds is proposed in an attempt to satisfy all the mechanical and physiological demands,[13] which are fabricated by combining two or more types of materials with selected properties, such as hydroxyl apatite, tri-calcium phosphates, fibers, and some other reinforced filler.[14,15] Nevertheless, the problems of interface compatibility along with biodegradability make this method complicated and sometimes impossible. In general situation, the structure and property of polymer materials are determined by processing technique. So far, to the best of our knowledge, no investigation is performed on balancing the requirements of both the mechanical performance and porosity of PLA scaffolds from the standpoint of novel fabrication method and controllable processing technology.

Current techniques for attaining porous PLA scaffolds mainly include salt leaching, phase separation, gas foaming, emulsion freeze-drying, and rapid prototype, to name just a few. PLA scaffolds fabricated by above methods are difficult to engineer clinically useful tissues and organs, which is attributed to the fatal drawbacks of inadequate mechanical properties in high load sharing situations.[16] High-pressure molding of polymers has gained wide attention over the past 40 years.[17–20] One of the reasons for the continuous focuses on this special processing way is that it can effectively improve the mechanical properties and thermal behavior of the resultant parts.[21,22] For instance, high pressure-modified high density polyethylene (HDPE) possessed extremely large values of the tensile strength ~260 MPa, nearly five times higher as compared with respect to the conventional HDPE.[23] As to the salt-leaching, its advantage resides in the pore size, porosity, and surface-to-volume ratio can be precisely controlled and readily manufactured. To prepare PLA scaffolds with sufficient mechanical stability and a well-defined network of interconnected pores, a novel fabrication approach named high-pressure compression molding/salt leaching was investigated in the current study. On the basis of this new processing technique, we first discussed the influence of composition on PLA scaffold properties, in the case porosity, morphology, thermal, and mechanical behaviors, and then the relationship between structural organization and comprehensive performance of the scaffolds was revealed. In addition, with the intent of further extending the application range of porous PLA scaffolds, the mechanical properties of scaffolds with optimized composition was further increased by modulating the processing temperature and pressure. It is of great interest to observe a remarkable improvement of PLA scaffolds' storage modulus, which even reaches up to 283.7 MPa and becomes the highest value ever reported in the literature. In the end, good cell proliferation within the fabricated scaffolds adequately demonstrates that the developed materials are well-suited candidates for the design of tailor-made matrices in bone tissue engineering.

MATERIALS AND METHODS

Materials

PLA (trade name 4032D), supplied by Nature Works, has the weight-average molecular weight $M_w = 1.17 \times 10^5$ g mol^{-1} and polydispersity $M_w/M_n = 1.6$. Calcium carbonate particles ($CaCO_3$, 2–8 μm in size) with a density of 2.7 g/cm^3 was purchased from Chengdu Kelong Chemical Reagent Factory (China) and was used as received.

Preparation of PLA/$CaCO_3$ Mixtures

Solution coagulation method was utilized to guarantee the good distribution of $CaCO_3$ in PLA. Taking PLA/$CaCO_3$ (10:90 wt/wt) mixture as an example, the detailed sample preparation was as follows: $CaCO_3$ (90 g) was added into 300 mL of CH_2Cl_2, and the solution was subjected to ultrasound and stir for 40 min to reach a uniform suspension. At the same time, 10 g of PLA was completely dissolved in 100 mL of CH_2Cl_2 by constant stirring. Then, the mixture solution was obtained by adding the CH_2Cl_2/PLA solution into the CH_2Cl_2/$CaCO_3$ suspension and continuously sonicated for another 40 min. Thereafter, C_2H_5OH (600 mL) was poured into the mixture solution until no more coagulated material precipitated. Finally, the precipitated mixture was transferred to blowing dryer, left overnight at 55°C, and dried in a vacuum oven at the same temperature for another 24 h to remove the traces of water. The PLA mixtures with content of $CaCO_3$ of 80, 90, 93, and 95 wt % were prepared.

High-Pressure Compression Molding

The self-made high-pressure compression molding apparatus is schematically shown in Figure 1(a). The diameter of the plunger is 20 mm, and the length of the cylindrical channel is 88 mm. Hydrostatic pressure supplied from a hydraulic jack can be up to 1 GPa, while the magnitude of pressure inside the channel can be measured via the modulated pressure meter with an accuracy of ±0.5 MPa, and the molding temperature is controlled via a thermocouple mounted 15 mm away from the channel, which ensures a temperature accuracy of 1°C inside the cell. The sample inside the channel was heated by an electrical heating sheath, which was controlled by a temperature controller. Prior to the experiment, the temperature of the inside channel was carefully calibrated with the *in situ* temperature measured by the thermocouple.

The temperature and pressure protocol is shown in Figure 1(b). At first, a given amount of PLA/$CaCO_3$ mixture was put inside the channel of the mold, heated to 165°C and kept the temperature for 30 min. After that a predetermined pressure of 640 MPa was applied to the sample during 2 min. Both the temperature and pressure were kept for 10 min to achieve a steady state. Then the material was cooled to room temperature at a rate of 2.5°C/min and released the pressure. To avoid the thermal degradation of PLA, we used nitrogen to protect the sample during the high-pressure compression molding. The size of the cylindrical parts obtained was 20 mm in diameter and 35 mm in height. The molded parts were cut into the rectangular specimens with dimensions of 35 × 10 × 4 mm^3 for the dynamic mechanical test. The interconnected porous structures were acquired by leaching the molded parts with low concentration ethylic acid for long enough time until the weight remained constant after dried in a vacuum oven, followed by immersing in distilled water 2 days to remove any residual solvent. Figure 2 illustrates the

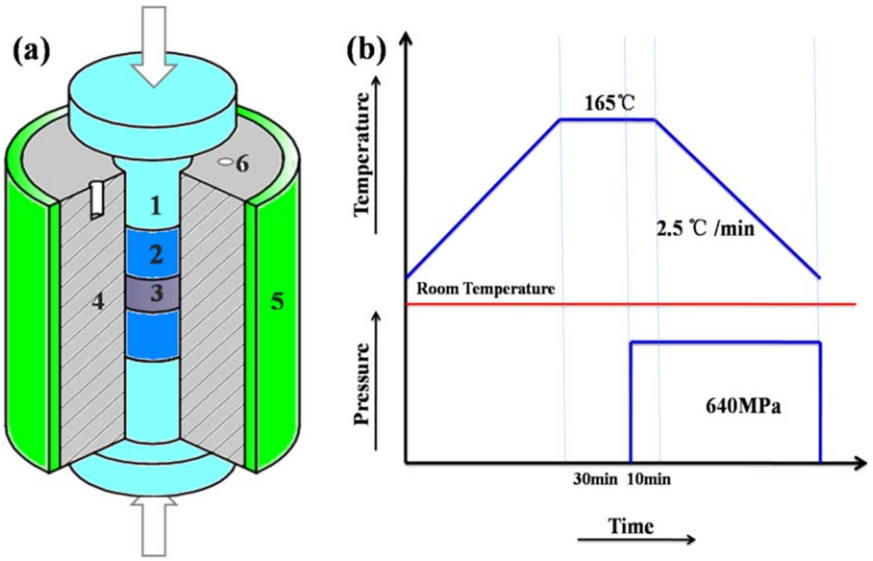

Figure 1. (a) Schematic of the high-pressure cell (1: Guide pillar; 2: Mold core; 3: Sample; 4: Mold; 5: Heater circle; 6: Thermocouple) and (b) temperature and pressure protocol. [Color figure can be viewed in the online issue, which is available at wileyonlinelibrary.com.]

detailed experimental procedures about the fabrication of porous PLA scaffolds as described above.

Characterization and Testing

SEM Images of the Scaffolds. Morphology of the porous PLA scaffolds was examined by a field emission scanning electron microscopy (SEM) (Inspect-F, FEI, Finland), operating in high vacuum and with an accelerating voltage of 20 kV. To expose the interior structure the specimens were frozen in liquid nitrogen for about 15 min, then quickly impact fractured. Prior to SEM examination the freshly broken surfaces were sputtered with gold.

Porosity, Connectivity, and Density of the Scaffolds. The quantitative estimation of the pore-related parameters of porous

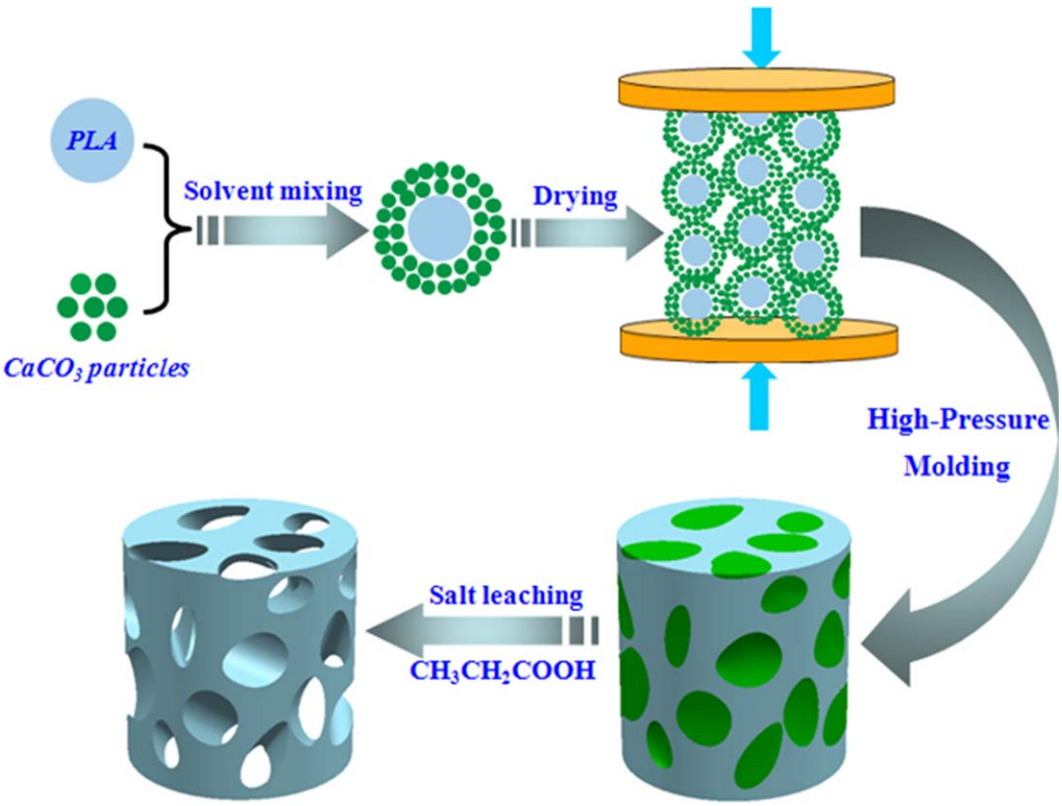

Figure 2. Schematic of fabrication procedures of porous PLA scaffolds. [Color figure can be viewed in the online issue, which is available at wileyonlinelibrary.com.]

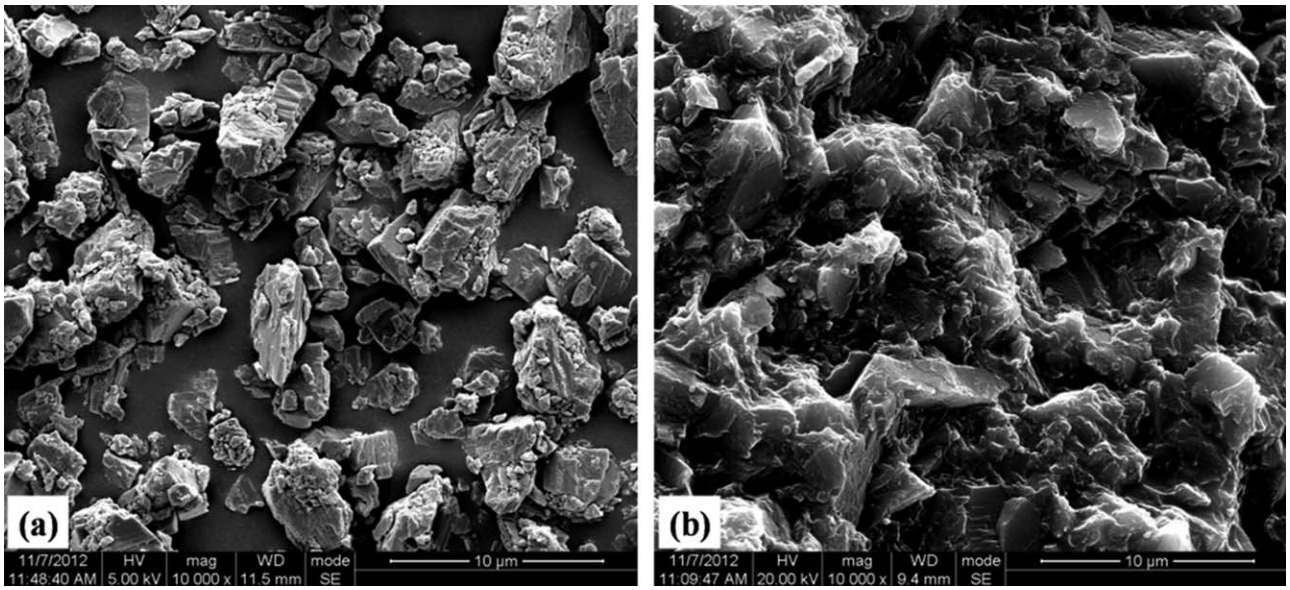

Figure 3. SEM micrograph of (a) pure $CaCO_3$ granules, (b) PLA/$CaCO_3$ (10 : 90 wt/wt) blends.

PLA scaffolds was performed via gravimetric measurements,[24] and the values of porosity, connectivity, and density were calculated as follows:

$$\text{Porosity} = \frac{m_{CaCO_3}/\rho_{CaCO_3}}{m_{CaCO_3}/\rho_{CaCO_3} + m_{PLA}/\rho_{PLA}} \times 100\% \quad (1)$$

$$\text{Connectivity} = \frac{m_0 - m'}{m_{0CaCO_3}} \times 100\% \quad (2)$$

$$\text{Density} = \frac{m'}{m_{CaCO_3}/\rho_{CaCO_3} + m_{PLA}/\rho_{PLA}} \times 100\% \quad (3)$$

where m_0 and m' are the mass of PLA/$CaCO_3$ mixtures before and after ethylic acid immersing, separately. m_{CaCO_3} equals to the difference of m_0 and m', while m_{0CaCO_3} represents the theoretical mass of $CaCO_3$ in PLA mixtures. The density (ρ) of $CaCO_3$ and PLA are 2.7 and 1.27 g/cm^3, respectively.

Thermal Properties of the Scaffolds. The melting behaviors of porous PLA scaffolds with different $CaCO_3$ contents were studied employing TA Q1000 V7.3 differential scanning calorimeter (DSC). The calibration was performed with indium and all tests were carried out in ultra pure nitrogen as purge gas. Samples (ca. 7 mg) enclosed in aluminum pans were heated from 40 to 190°C at a scanning rate of 10°C/min. Melting point temperatures were determined from the melting curves as peak temperatures. The fractional crystallinity (X_c %) was calculated by using the equation as follows.

$$\chi_c = \frac{(\Delta H_{cc} + \Delta H_m)}{\Delta H_0} \times 100\% \quad (4)$$

where ΔH_{cc} is the cold crystalline enthalpy; ΔH_m is the melting enthalpy; ΔH_0 is the melting enthalpy of 100% crystalline PLA, which is set as 93 J/g in this study.[25]

Crystal Structure of the Scaffolds. The wide-angle X-ray diffraction (WAXD) measurements were conducted on the synchrotron light source under room temperature in the National Synchrotron Radiation Laboratory (NSRL), Hefei. The distance from sample to detector was 250 mm, the wavelength of the monochromated X-ray was 0.15418 nm, and the beam size is about 400 μm. Then the 2D-WAXD images were collected with an X-ray CCD detector (Model Mar345). An aluminum oxide (Al_2O_3) standard was used to calibrate the scattering angle for WAXD, and air scattering was subtracted. Linear WAXD profiles were obtained from circularly integrated intensities of 2D-WAXD image patterns acquired, Gaussian functions were applied to fit the amorphous background, and an iterative peak-fit procedure was used to fit the crystalline reflections of WAXS profiles. The intensity was plotted as a function of the scattering vector, q, where $|q| = 4\pi(\sin\theta)/\lambda$, λ is the wavelength of the incident beam, and 2θ is the scattering angle. Subsequently, through deconvoluting the peaks of linear WAXD profiles, the overall crystallinity X_c was calculated by

$$\chi_c = \frac{\sum A_{cryst}}{\sum A_{cryst} + \sum A_{amorp}} \quad (5)$$

where A_{cryst} and A_{amorp} are respectively the fitted areas of crystal and amorphous.

Mechanical Properties of the Scaffolds. DMA characterization was carried out using a Q800 DMA instrument (TA, America) in a three point bending mode with a dual cantilever clamp (the ASTM standard D4065). And the apparatus was operated with a heating rate of 3°C/min^{-1} from 30 to 160°C. Rectangular samples (35 × 10 × 4 mm^3) were submitted to an oscillatory deformation at a frequency of 1 Hz.

Cell Culture Tests of the Scaffolds. PLA scaffolds used for cell culture tests were sterilized using ethylene oxide gas, and then washed with excess phosphate buffered saline (PBS). Fibroblasts cells (L929 cells) were seeded onto the prepared scaffolds in 12-well plates at a density of 100,000 cells/well, and the scaffolds were immobilized in culture dishes at 37°C in 5% of CO_2. A Termanox

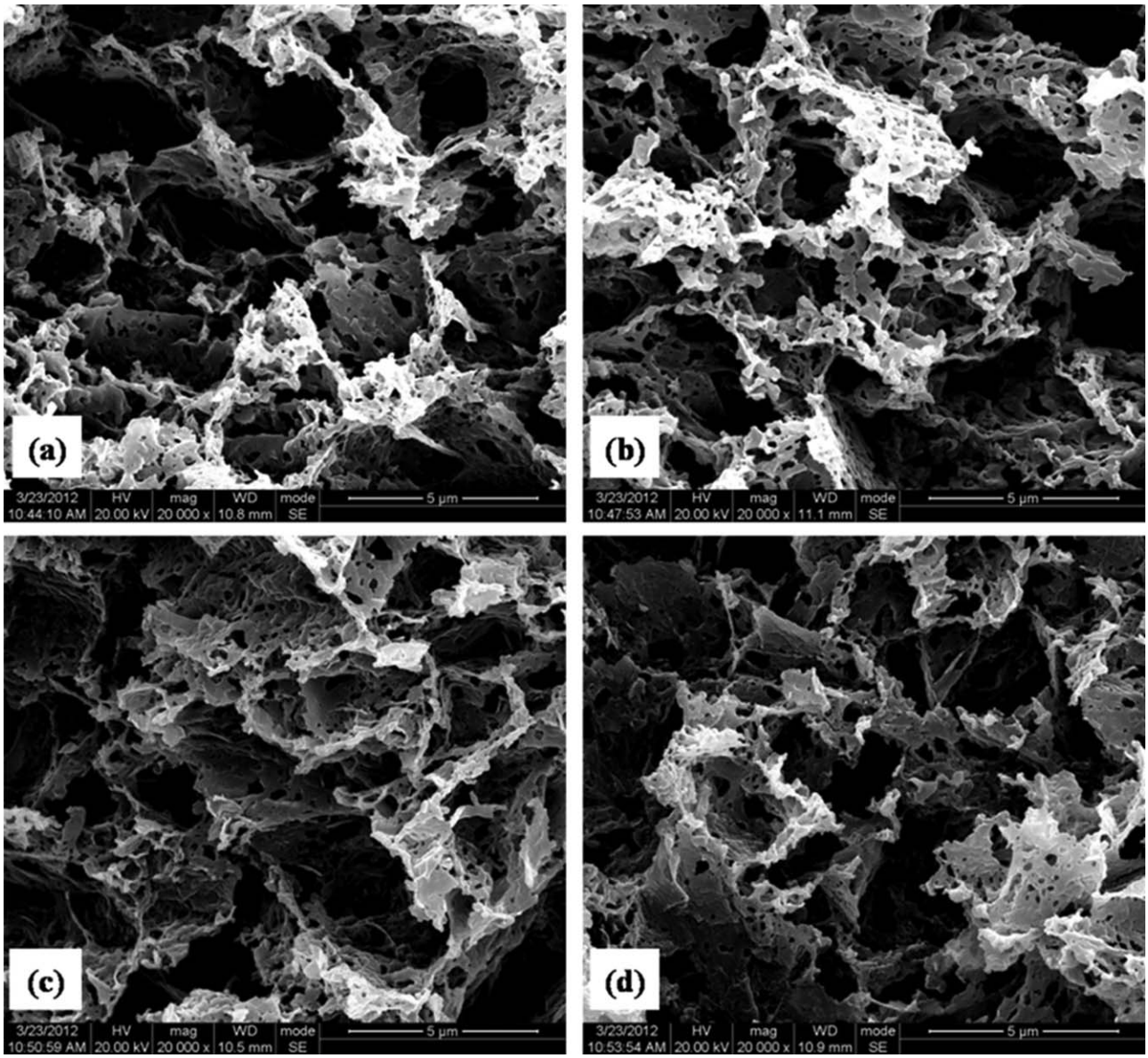

Figure 4. SEM micrograph of porous PLA scaffolds with different $CaCO_3$ contents: (a) PLA/$CaCO_3$ (5 : 95 wt/wt); (b) PLA/$CaCO_3$ (7 : 93 wt/wt); (c) PLA/$CaCO_3$ (10 : 90 wt/wt); and (d) PLA/$CaCO_3$ (20 : 80 wt/wt).

plastic plate was used as a control sample and the α-MEM containing 10% FBS was used as the culture medium, and it was changed every day after culture. The morphology of the cells cultured on scaffolds was observed by SEM. The cells cultured for 3 days were fixed with 2.5% glutaraldehyde in PBS for 2 h at 4°C. After they had been thoroughly washed with PBS, the samples were dehydrated sequentially through a series of increasing concentrations of ethanol (10%, 30%, 50%, 70%, 80%, 90%, 95%, and 100%) for 15 min ×2. Finally, scaffolds were critical-dried with hexamethyldisilazane, coated with Au, and examined with SEM.

RESULTS AND DISCUSSION

Determination of the Optimized Composition of the Scaffolds

Figure 3(a) presents the typical morphology of as-received $CaCO_3$ granules, which are characterized by rectangular in shape with a number average grain size of 5.5 μm, and size of the particles ranges from 2 up to 8 μm. Figure 3(b) indicates the gross morphology of PLA/$CaCO_3$ (10:90 wt/wt) mixture formed after high-pressure compression molding. It can be seen that there is no significant difference of domain size between PLA and $CaCO_3$ phases, and both of them are fully continuous. Formation of the cocontinuous structure is mainly attributed to two aspects. Firstly, high content of $CaCO_3$ is apt to agglomerate and connect. Furthermore, the flowable PLA has great tendency to be the continuous phase when pressure exerts.[26] As shown in Figure 4, a great number of three-dimensional connected open pores are homogeneously distributed in PLA skeleton, with pore diameters falling in the range of 2.5–10.8 μm. After immersing the mixtures in low concentration ethylic acid, the space originally occupied by $CaCO_3$ becomes pores, and the PLA phase is still self-supporting, thus formed the final porous

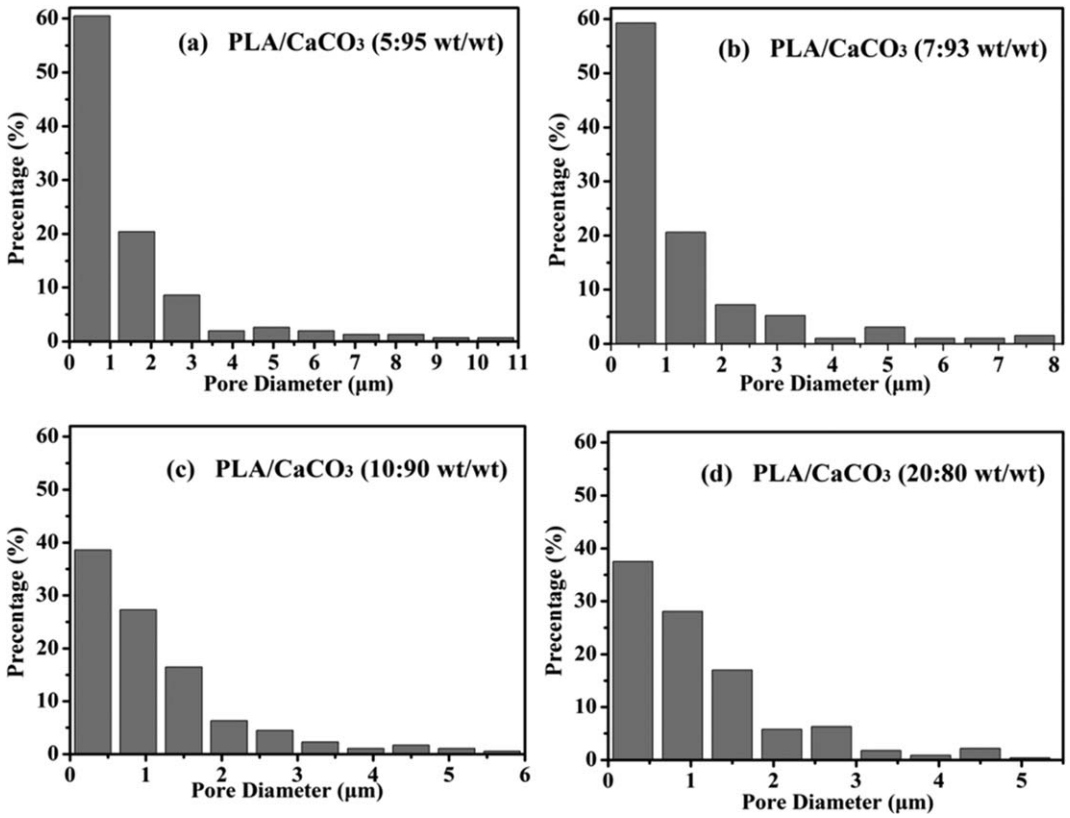

Figure 5. The distribution of pore size of porous PLA scaffolds with different $CaCO_3$ contents: (a) PLA/$CaCO_3$ (5 : 95 wt/wt); (b) PLA/$CaCO_3$ (7 : 93 wt/wt); (c) PLA/$CaCO_3$ (10 : 90 wt/wt); and (d) PLA/$CaCO_3$ (20 : 80 wt/wt).

scaffold structure. This treatment ensures the complete connectivity of pores in the scaffolds because of the dissolution of continuous $CaCO_3$ phase. The interconnected pore structure should be able to provide enough space for possible vascularization when being implanted, and such the low pore size endows the porous scaffolds high specific surface areas. While, except for many interconnected pores, some circular pores with smaller sizes (1–2 μm) can also be observed on pore walls, indicating that some low levels of $CaCO_3$ remain as dispersed droplets in the PLA skeleton before leaching.[27] These tiny pores will not only act as the channel to transport nutrients or metabolism product, but also make the pore walls more rougher, which could be beneficial to improve the interfacial adhesion between cells and scaffold matrix, so that further promotes the attachment and growth of cells.[28,29] From the micrographs, we can draw a conclusion that the well-defined porous PLA scaffolds can be successfully fabricated by using the high-pressure compression molding/salt leaching method.

It is well accepted that the microstructure such as pore size and its distribution, porosity as well as pore shape has prominent influence on cell intrusion, proliferation, and function in tissue engineering. Figure 5 reveals the evident morphological differences in pore size and its distribution between different compositions. With the increase of $CaCO_3$ contents, larger and more pores are obtained together with a higher pore density; however, at the cost of destroying the uniformity of pores distribution. This trend can be seen from the porous PLA scaffolds (PLA/$CaCO_3$-5 : 95 wt/wt), in which the average pore size is on the order of 5.5 μm, to the porous PLA scaffolds (PLA/$CaCO_3$- 20 : 80 wt/wt), where lower average pore sizes of 2.5μm and narrower pore size distribution are observed. This property could be attributed to $CaCO_3$, which acts as the porogen, high content of which is easy to lead to the fusion of smaller pores to generate larger ones and then broaden the pores scope.

Pore-related parameters of porous PLA scaffolds are shown in Table I. Porosity is often created in solid scaffold by the inclusion of porogen that can be leached away upon placement in an aqueous environment,[30] which reflects the volume fraction of pores as compared with the total volume of scaffold. It is worthy to notice that the porosity of all prepared scaffolds is higher than 60%, well meeting the requirements of application in tissue engineering.[31–33] More interestingly, the porosity increases dramatically from 65.06% to 89.75% as $CaCO_3$ increases from 80 to 95 wt %, so that the PLA scaffolds could provide more space to guide cell attachment and proliferation.[34] On the basis of above results, one can deduce that porosity is dependent on the salt/polymer ratio in high-pressure compression molding/salt leaching technique, that is, the more content of $CaCO_3$ in mixture the higher porosity of porous PLA scaffolds. Unlike the changes of porosity, variation of the composition has no detectable effect on the pore interconnectivity of the formed scaffolds, and its values nearly equal to 99%, which demonstrates that $CaCO_3$ within the mixtures is fully continuous. The highly interconnected porous materials can be easily seeded with a fluid phase containing cells, for it is desirable for permitting cell infiltration into and throughout the scaffolds. In addition, it is

Table I. Porosity, Connectivity, and Density of Scaffolds with Different Contents of $CaCO_3$

PLA/$CaCO_3$	m_0 (g)	m' (g)	m_{CaCO_3} (g)	m_{0CaCO_3} (g)	Porosity (%)	Connectivity (%)	Density (g/cm^3)
5/95	1.73	0.09	1.64	1.643	89.75	99.79	0.133
7/93	1.60	0.12	1.48	1.488	85.73	99.46	0.188
10/90	1.45	0.15	1.30	1.305	80.59	99.62	0.251
20/80	1.33	0.27	1.06	1.064	65.06	99.62	0.447

m_0 indicates quality of PLA/$CaCO_3$ mixtures before ethylic acid immersing, while m', represents the mass of porous PLA scaffold after solvent casting. m_{CaCO_3} equals to the subtraction of m_0 and m', m_{0CaCO_3} means the theoretical quality of $CaCO_3$, moreover, the density of $CaCO_3$ and PLA are 2.7 and 1.27 g/cm^3, respectively. Porosity, connectivity, and density of the scaffolds were determined by gravimetric measurements according to eqs. (1)-(3), separately.

well acknowledged that all kinds of porogens could not be completely removed even immersed in good solvent for long enough time. The residual porogens may have a negative effect on tissue regeneration. However, $CaCO_3$ is served as a bioresorbable inorganic substance and has been used clinically as bone filler, showing excellent bone-forming ability, biodegradability, and biocompatibility.[35] A little residue of it will lead to the formation of the alkaline environment, so as to facilitate the growth of cells instead of doing harm to human's body.[36] In terms of density obtained by weighing a sample of specific volume, it exhibits a downward trend with increasing of $CaCO_3$ content. Especially, when the content increases to 95 wt %, it is just 0.133 g/cm^3, nearly the lowest density reported so far for porous scaffolds at such a high porosity and connectivity,[37] fully embodying the scaffolds prominent superiority of being lightweight.

In biomedical applications, any PLA-based implanted material will be in the glassy state,[38] for the glass transition temperature (T_g) of PLA (60–65°C) is above the physiological temperature (~37°C). Nevertheless, as T_g is not far from 37°C, PLA will slowly approach the equilibrium at this temperature, during which the occurrence of structural relaxation or physical aging would bring about the poor heat resistance and structural stability of PLA scaffolds.[39,40] To our great surprise, thermal analysis reveals that the as-obtained porous PLA scaffolds for each composition have an extremely high T_g around 84°C (see Figure 6), nearly 20°C higher as compared to conventional compression molded PLA. Such a significant increase means a remarkable improvement of PLA scaffolds' ability to resist deformation. There exist two factors influencing the glass transition dynamics of PLA: crystallinity and high pressure effect. On one hand, the crystallinity of high-pressure compression molded PLA is all above 40% through DSC measurements, obviously superior to those by conventional processing technologies such as extrusion and injection-molding. The high crystallinity generates significant volume reduction and shrinkage, and then the crystalline regions constrain the amorphous phase and influence the conformational motions of molecular chains.[41] On the other hand, it is well-known that T_g increases with pressure and its sensitivity to pressure dT_g/dP has been found to lie between 0.015 and 0.03 K/MPa for a wide variety of amorphous and semicrystalline polymers,[42] which is mainly related to the condensed free volume and restricted molecular movement.[43] During the high-pressure compression molding process, the ability

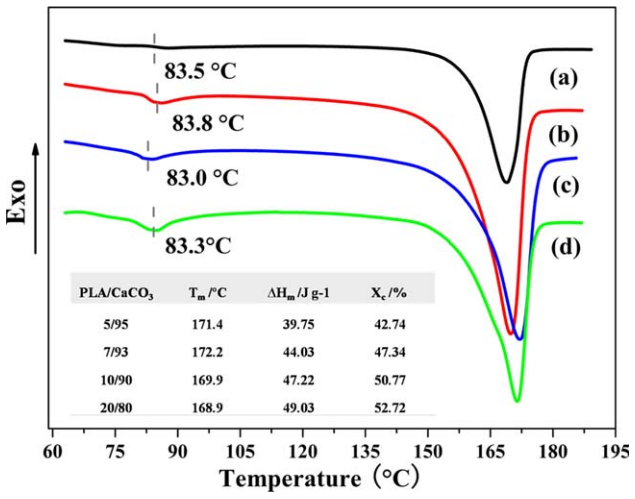

Figure 6. DSC schemes of porous PLA scaffolds with different $CaCO_3$ contents: (a) PLA/$CaCO_3$ (20 : 80 wt/wt); (b) PLA/$CaCO_3$ (10 : 90 wt/wt); (c) PLA/$CaCO_3$ (7 : 93 wt/wt); and (d) PLA/$CaCO_3$ (5 : 95 wt/wt). [Color figure can be viewed in the online issue, which is available at wileyonlinelibrary.com.]

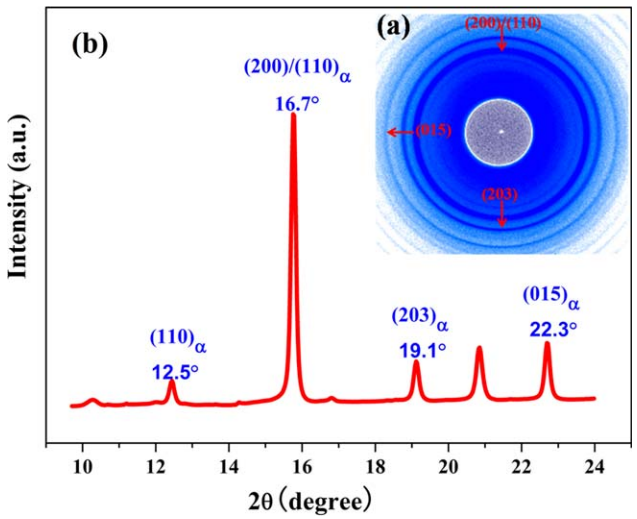

Figure 7. Representative (a) WAXD patterns and (b) corresponding 1D WAXD curves of porous PLA scaffolds (PLA/$CaCO_3$-10 : 90 wt/wt). [Color figure can be viewed in the online issue, which is available at wileyonlinelibrary.com.]

of polymer chains to conform to the normal low temperature configuration is constrained, and this restraint effect continuously maintained until exhibited as a result that the glass structure is attained at a higher temperature.[44] Moreover, glass transition temperature and melting temperature of PLA scaffolds nearly remain unchanged for different compositions, suggesting that the influence of composition on PLA scaffolds' thermal properties is insignificant over the filler range studied.

Wide-angle X-ray diffraction measurement was performed to determine the crystalline structure of PLA scaffolds, and the data was collected over the 2θ range from 10° to 24°. XRD pattern (see the inset in Figure 7) of the fabricated porous scaffolds elaborates the highly crystalline nature of PLA, quantified by the crystallinity of 49.8% calculated by deconvoluting the peaks of linear WAXD profiles. As is evident from the figure, the profile shows strong diffraction peaks at 2θ = 16.7°, 19.1°, 12.5°, and 22.3° assigned to the diffraction planes (200)/(110), (203), (110), and (015) of the stable α-form of PLA crystals, respectively. Until now, three different crystalline modifications (α, β, γ) of PLA are identified upon changing the preparation conditions. The α-form is believed to grow from the melt or cold solution under normal conditions, with a 10_3 helical chain conformation in which two chains interact to form an orthorhombic unit cell. The β-form is prepared at a high draw ratio and is known to take a left-handed 3_1 helical conformation, whereas a new γ-form produced through epitaxial crystallization was described by Cartier et al.[45] Among these crystalline modifications, stable α-form is preferred, because of its relatively ordered crystalline structures and the highest melting point (180°C).[46,47] To this end, the existence of only α-crystals in our porous scaffolds implies the formation of crystallites with good tacticity and stability. The high crystallinity gained in WAXD measurements is well in line with the DSC results, which may due to some contribution of high pressure in facilitating formation of crystallites and enhancing crystallization ability.

Dynamic mechanical analysis (DMA) has been proved to be effective in detecting the thermal mechanical properties and mobility of chain segments.[48] Figure 8 illustrates the storage modulus (E'), loss modulus (E''), and loss factor (tanδ) of porous PLA scaffolds as a function of temperature. With regard to the porous scaffolds (PLA/$CaCO_3$-20 : 80 wt/wt), they displays strong ability to resist deformation with the storage modulus high up to 132.3 MPa. Noticeably, in comparison with the maximal value (107.5 MPa) of the scaffolds once reported with similar porosity and composition,[49,50] it is still 25 MPa higher, which represents an encouraging progress in developing load-bearing scaffolds. While with the increasing porosity, the storage modulus of scaffolds (PLA/$CaCO_3$-7 : 93 wt/wt) declines to 12.7 MPa. It is apparent that the storage modulus of PLA scaffolds has a close relationship with compositions. This is because at high porosity, pore walls are too thin to transfer the applied stress effectively, and finally leads to the decrease of carrying capacity of scaffold. Thus, we can make a conclusion that the pores seem to act as defects, which undermine the stiffness of scaffolds, to obtain the scaffolds with high resistence to external load the choice of $CaCO_3$ content needs to be appropriate. The effect of porosity on loss modulus (E'') and loss factor (tanδ) is

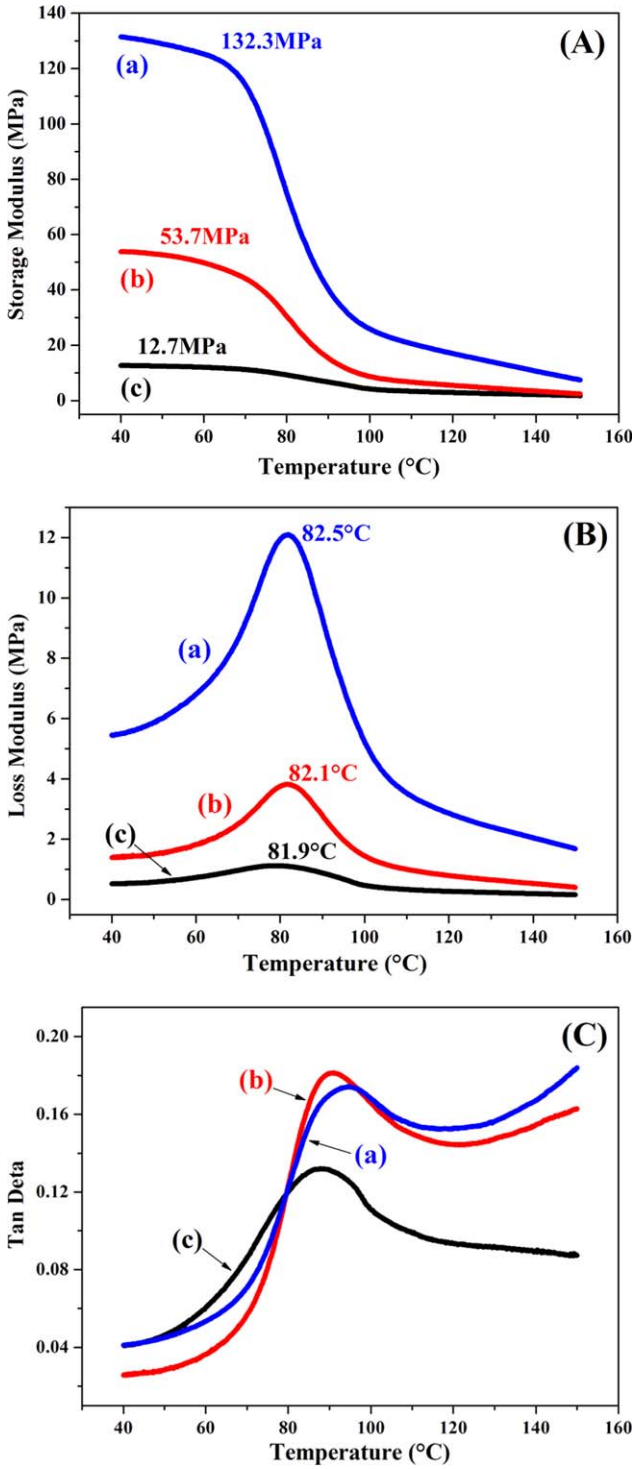

Figure 8. Temperature dependence of storage modulus (E'), loss modulus (E''), and loss factor (tan δ) for porous PLA scaffolds formed under 165°C and 640 MPa: (a) PLA/$CaCO_3$ (20 : 80 wt/wt); (b) PLA/$CaCO_3$ (10 : 90 wt/wt); and (c) PLA/$CaCO_3$ (7 : 93 wt/wt). [Color figure can be viewed in the online issue, which is available at wileyonlinelibrary.com.]

exhibited in Figure 8(b,c), respectively. As can be seen, E'' and tanδ are both the lowest when $CaCO_3$ content increases to 93 wt %. Conformation transition always exists in the course of glass transition as well as high-temperature relaxation, which is

mainly related with the imperfect elasticity of polymers.[51] It is generally believed that E'' and tanδ in the transition region mainly measures the physical loss of macromolecules. The amount of PLA in the scaffolds will deduce as $CaCO_3$ grow in quantity, consequently, values of E'' and tanδ also exhibit a declining trend. The glass transition temperature (T_g) of PLA scaffolds for all compositions is defined as the temperature where the loss modulus reaches a maximum as shown in Figure 8(b). It is interesting that the scaffolds exhibits an increase in T_g about 20°C as compared to the conventional processed PLA. This kind tremendous augment verified via DMA, is also shown in the first heating ramp through DSC measurements as given in Figure 6, which again confirms the prominent improvement on the heat resistance and structural stability of our fabricated porous PLA scaffolds.

As aforementioned, porosity of PLA scaffolds increases significantly with $CaCO_3$ contents so that a high density of cells would be seeded. However, the mechanical strength of PLA scaffolds would undoubtedly suffer at the same time, because the massive interconnected open pores do damage to materials' stiffness along with the carrying capacity. Considering the requirements of scaffold design on both mechanical and structural aspects, the overall properties of porous PLA scaffolds will be optimal when the content of $CaCO_3$ is 90 wt %. Its porosity, density, and storage modulus are 80.59%, 0.251 g/cm^3 and 53.7 MPa, respectively, not only satisfying the physiological demands to guide cell ingrowth for tissue formation, but also maintaining a sufficient strength to ensure the integrity of scaffold structure.

Improved Mechanical Performance by Regulating Processing Techniques

One of the main problems in tissue engineering is designing suitable scaffolds that meet the demands for application in "hard mineralized tissues," such as bone.[52] It is generally accepted that the scaffold material should have mechanical strength as close as possible to the strength of the bone to be repaired or substituted. While unfortunately, the storage modulus of porous scaffolds reported to date is far away from the criterion exhibited by the scaffolds fall in the normal range of trabecular bone,[24,53] which is about 50–250 MPa.[25] To address this issue, we first attempt to achieve a highly densified porous structure by regulating the processing technique. Figure 9(a,b) depicts the storage modulus (E') of PLA scaffolds formed under different molding temperature and pressure, the values of them are summarized in Figure 9(c). As expected, a noteworthy promotion in storage modulus is achieved with increasing temperature and pressure. Especially, when the temperature is 190°C, the high pressure of 1000 MPa gives rise to a considerable improvement of storage modulus, which changes from 19.7 MPa up to a superb level of 283.7 MPa, approximately 15 times higher in comparison with the low-pressure compression molded scaffolds. Actually, the porous PLA scaffolds fabricated under this situation completely comply with the normal requirements in bone tissue engineering.

To elucidate the effect of processing technique on the mechanical property of PLA scaffolds, we carefully examined their microstructure. Morphology of fractured surfaces of PLA scaffolds prepared under different temperatures and pressures is displayed in Figure 10. Figure 10(a) shows the porous structure of scaffolds fabricated under 165°C and 5 MPa. A great number

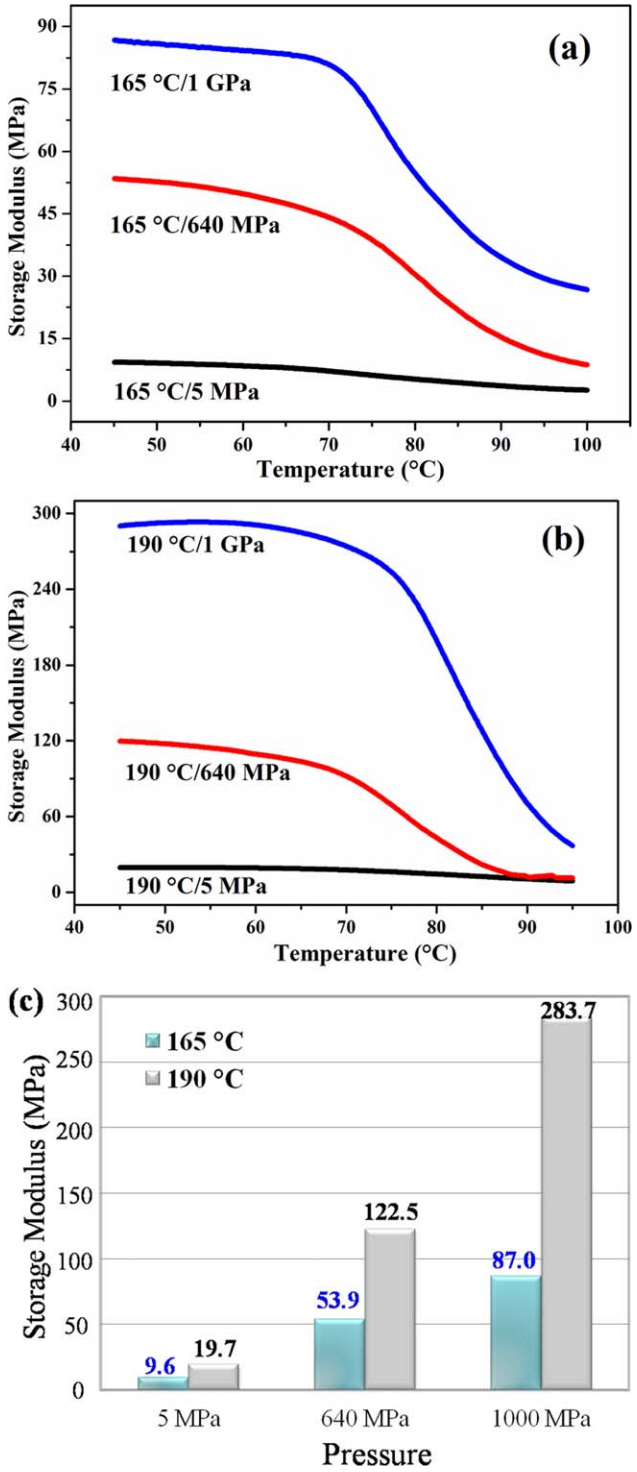

Figure 9. DMA schemes (a, b) of porous PLA scaffolds formed in different process conditions and E′-T-P scheme (c) of porous PLA scaffolds formed in different process conditions. [Color figure can be viewed in the online issue, which is available at wileyonlinelibrary.com.]

Applied Polymer SCIENCE

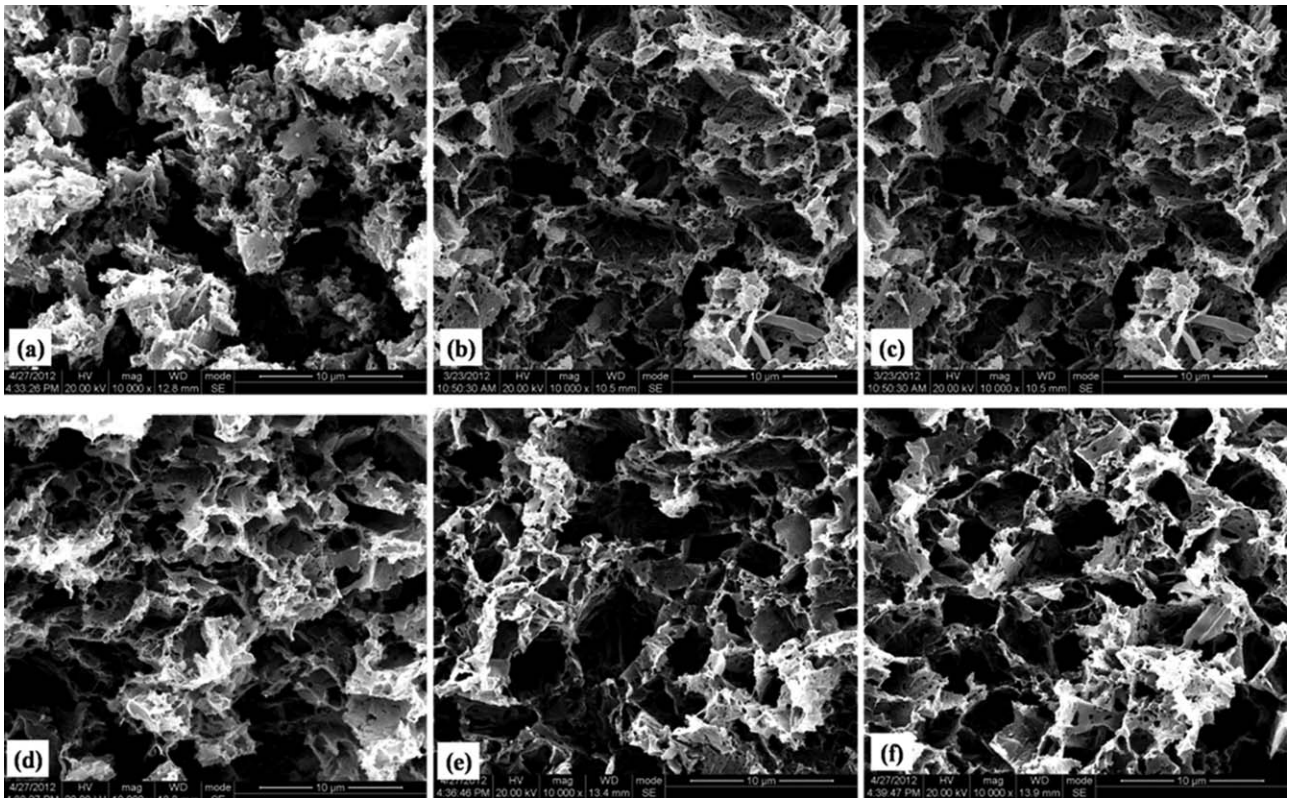

Figure 10. SEM schemes of porous PLA scaffolds formed in different process conditions: (a) 165°C/5 MPa; (b) 165°C/640 MPa; (c) 165°C/1000 MPa; (d) 190°C/5 MPa; (e) 190°C/640 MPa; and (f) 190°C/1000 MPa.

of interconnected open pores with irregular shape throughout and unevenly distributed in PLA skeleton, and the skeleton exists in the form of isolated individuals, suggesting a weak interaction adhesion between them. Under this circumstance, as long as external force applied to the scaffolds, stress could not effectively convey so that the structure of scaffolds is prone to be collapsed. On the contrary, according to scaffolds formed under 190°C and 1000 MPa [see Figure 10(f)], an interconnected three-dimensional network structure is observed, which believes to be indispensable in load bearing for the stable interconnections between pores.[54] Above morphology difference indicates that high temperature and pressure are beneficial to

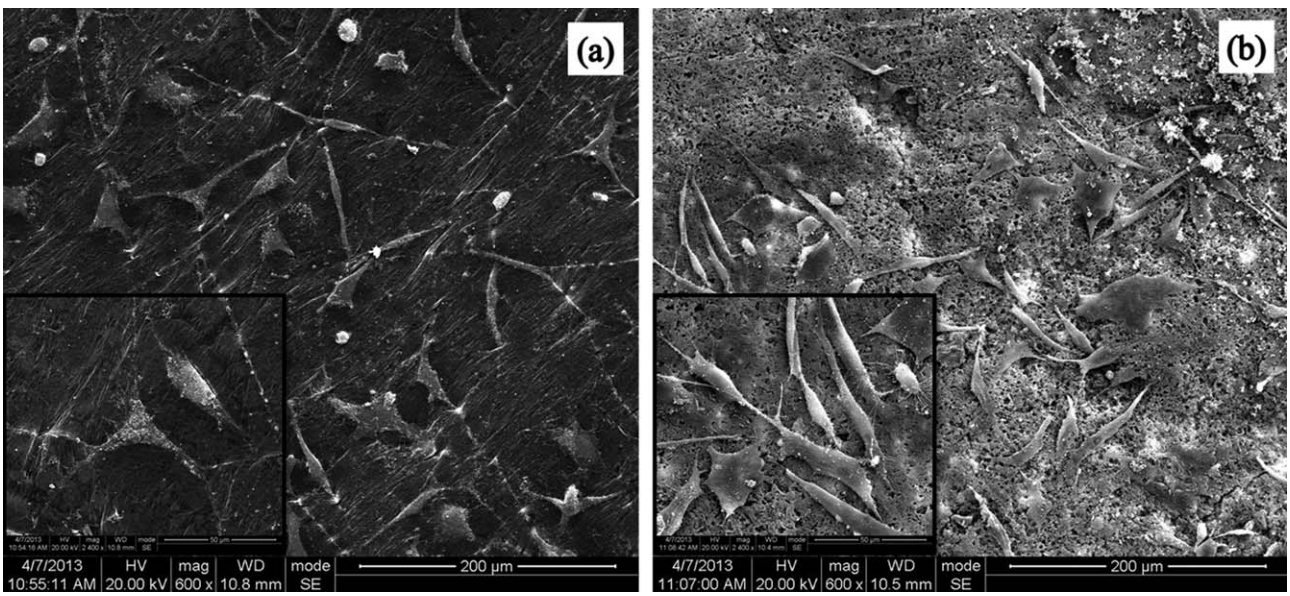

Figure 11. SEM micrograph of (a) Termanox plastic plate and (b) porous PLA scaffolds after culturing fibroblasts cells (L929) for 3 days.

acquire PLA scaffolds with strong mechanical property, because the mobility of PLA molecular chains enhances with the increase of temperature and pressure, thereby resulting in more compact and stronger intermolecular forces in scaffolds.

Proliferation of Fibroblasts Cells (L929 Cells) on the Scaffolds

Attachment and growth of cells are critical for scaffolds to guide the regeneration of tissue, and so the ability of cells to proliferate within these scaffolds was evaluated. Cytotoxicity and relative cell viability of PLA scaffolds fabricated under 190°C/1000 MPa were observed by SEM morphology of fibroblasts cells. Similar with the situation in Termanox plastic plate [Figure 11(a)], cells seeded on scaffolds [Figure 11(b)] adhere on the pore walls tightly with typical shuttle-like morphology, spread throughout within the scaffolds in a three-dimensional fashion, and be surrounded by a fibrous extracellular matrix. It is well-known that cells have a favorable growth state in plastic plate, the result comparable to the control sample fully verifies a good adhesion between PLA scaffolds and fibroblasts cells, suggesting our scaffolds *possess* high cellular compatibility and can effectively accelerate cell infiltration and proliferation.

CONCLUSIONS

In this work, it is demonstrated for the first time that the porous PLA scaffolds can be successfully prepared by the proposed high-pressure compression molding/salt leaching method. By doing the analysis of data derived from SEM, DSC and DMA, we made a conclusion that when the content of porogen ($CaCO_3$) was 90 wt %, the PLA scaffolds were not only with an interconnected open pore structure, but also highly porous with porosity larger than 80%. It was truly interesting that the structural stability of high-pressure molded scaffolds was remarkably improved based on the fact that its glass transition temperature (83.5°C) increased about 20°C, as compared to that of the conventional compression-molded PLA (60°C), which is not far from physiological temperature (~37°C) at the risk of structural relaxation or physical ageing. To further extend the practical application range of porous PLA scaffolds, *a* superb level of 283.7 MPa of the storage modulus was achieved by optimizing the processing temperature and pressure, significantly improved compared with the maximal value (107.5 MPa) of PLA scaffolds once reported with similar porosity and composition. Additional, the applicability to cell culture of the scaffolds with optimal compositions and process parameter has also been examined. It was observed that the fibroblasts cells cultured in scaffolds could attach, spread, and proliferate well, indicates measures of regulating high-pressure processing technique to improve mechanical properties without sacrificing other properties (biocompatibility, porosity, and osteoconductivity) are highly desirable. To this end, future studies will involve the optimization of tissue growth within the porous matrices and *in vivo* testing of the scaffold materials.

ACKNOWLEDGMENTS

National Natural Science Foundation of China, 51120135002, 51121001; National Outstanding Youth Foundation of China, 50925311.

REFERENCES

1. Hutmacher, D. W. *Biomaterials* **2000**, *21*, 2529.
2. Ravati, S.; Favis, B. D. *Polymer* **2011**, *52*, 718.
3. Sikavitsas, V. I.; Temenoff, J. S.; Mikos, A. G. *Biomaterials* **2001**, *22*, 2581.
4. Gong, X.; Tang, C. Y.; Zhang, Y.; Wong, C. T.; Wu, S.; Liu, J. *J. Appl. Polym. Sci.* **2012**, *125*, 571.
5. Molamma, P.; Prabhakaran, A.; Sreekumaran, N.; Dan, K.; Seeram, R. *Biopolymers* **2012**, *97*, 529.
6. Blaker, J. J.; Maquet, V.; Jérôme, R.; Boccaccini, A. R.; Nazhat, S. N. *Acta Biomater.* **2005**, *1*, 643.
7. Kothapalli, C. R.; Shaw, M. T.; Wei, M. *Acta Biomater.* **2005**, *1*, 653.
8. Mikos, A. G.; Temenoff, J. S. *Electron. J. Biotechnol.* **2000**, *3*, 114.
9. Bleach, N. C.; Nazhat, S. N.; Tanner, K. E.; Kellomaki, M.; Tormala, P. *Biomaterials* **2002**, *23*, 1579.
10. Chen, G. P.; Ushida, T.; Tateishi, T. *Biomaterials.* **2001**, *22*, 2563.
11. Deng, Y.; Zhao, K.; Zhang, X.; Hu, P.; Chen, G. Q. *Biomaterials* **2002**, *23*, 4049.
12. Jun, S. L.; Chang, S. K.; Jong, W. K.; Kwang, G. L.; Seok, W. K.; Hae, Y. K.; Young, H. P. *Biopolymers* **2011**, *97*, 265.
13. Han, W. W. T.; Misra, R. D. K. *Acta Biomater.* **2009**, *5*, 1182.
14. Kweon, H. Y.; Yoo, M. K.; Park, I. K.; Kim, T. H.; Lee, H. C.; Lee, H. S. *Biomaterials* **2003**, *24*, 801.
15. Alireza, S.; Sarvestani, X. H.; Esmaiel, J. *Biopolymers* **2006**, *85*, 370.
16. Ma, P. X.; Choi, J. W. *Tissue Eng.* **2001**, *7*, 23.
17. Tseng, H. T.; Phillips, P. J. *Macromolecules* **1985**, *18*, 1565.
18. Saeki, S.; Takei, S.; Ookubo, Y.; Tsubokawa, M.; Yamaguchi, T.; Kikegawa, T. *Polymer* **1998**, *39*, 4267.
19. Dimeska, A.; Phillips, P. J. *Polymer* **2006**, *47*, 5445.
20. Fuss, T.; Milankovic, A. M.; Ray, C. S.; Lesher, C. E.; Youngman, R.; Day, D. E. *J. Non-Cryst. Solids* **2006**, *352*, 4101.
21. Sorrentino, A.; Pantani, R.; Titomanlio, G. *Macromol Res.* **2010**, *18*, 1045.
22. Yu, J. C.; Gröbner, G.; Tonpheng, B.; Andersson, O. *Polymer* **2011**, *52*, 5521.
23. Beloshenko, V. A.; Askadskii, A. A.; Varyukhin, V. N. *Russ. Chem. Rev.* **1998**, *67*, 951.
24. Guarino, V.; Causa, F.; Taddei, P.; Foggia, M. D.; Ciapetti, G.; Martini, D.; Fagnano, C.; Baldini, N.; Ambrosio, L. *Biomaterials* **2008**, *29*, 3662.
25. Sarazin, P.; Roy, X.; Favis, B. D. *Biomaterials* **2004**, *25*, 5965.
26. Sarazin, P.; Favis, B. D. *Biomacromolecules* **2003**, *4*, 1669.
27. Yuan, Z.; Favis, B. D. *AIChE J.* **2004**, *25*, 2161.
28. Williams, J. M.; Adewunmi, A.; Schek, R. M.; Flanagan, C. L.; Krebsbach, P. H.; Feinberg, S. E.; Hollister, S. J.; Das, S. *Biomaterials* **2005**, *26*, 4817.

29. Ferdous, J.; Kolachalama, V. B.; Shazly, T. *Acta Biomater.* **2013**, *9*, 6052.
30. Kang, Y. Q.; Yin, G. F.; Yuan, Q.; Yao, Y. D.; Huang, Z. B.; Liao, X. M. *Mater. Lett.* **2008**, *62*, 2029.
31. Shieh, Y. T.; Liu, G. L. *J. Polym. Sci. Part B: Polym. Phys.* **2007**, *45*, 466.
32. Thmenoff, J. S.; Mikie, A. G. *Biomaterials* **2000**, *21*, 431.
33. Kim, B. S.; Mooney, D. J. *Trends Biotechnol.* **1998**, *16*, 224.
34. Jones, J. R.; Hench, L. L. *Curr. Opin. Solid Mater.* **2003**, *7*, 301.
35. Zheng, L. Q.; Yang, F.; Shen, H.; Hu, X. F.; Mochizuki, C.; Sato, M.; Wang, S. G.; Zhang, Y. D. *Biomaterials* **2011**, *32*, 7053.
36. Obata, A.; Hotta, T.; Wakita, T.; Ota, Y.; Kasuga, T. *Acta Biomater.* **2009**, *6*, 1248.
37. Guo, C.; Guo, X.; Cai, N.; Dong, Y. S. *Mater. Lett.* **2012**, *74*, 197.
38. Mano, J. F.; Ribelles, J. L. G.; Alves, N. M.; Sanchez, M. S. *Polymer* **2005**, *46*, 8258.
39. Li, H. B.; Huneault, M. A. *Polymer* **2007**, *48*, 6855.
40. Sant, S.; Iyer, D.; Gaharwar, A. K.; Patel, A.; Khademhosseini, A. *Acta Biomater.* **2013**, *9*, 5693.
41. Lee, J. H.; Park, T. G.; Park, H. S.; Lee, D. S.; Lee, Y. K.; Yoon, S. C.; Nam, J. D. *Biomaterials* **2003**, *24*, 2773.
42. Wang, F.; Saeki, S.; Yamaguchi, T. *Polymer* **1997**, *38*, 3485.
43. Castagnet, S.; Thilly, L. *J. Polym. Sci. Part B: Polym. Phys.* **2009**, *47*, 2015.
44. Thirtha, V.; Lehman, R.; Nosker, T. *Polymer* **2006**, *47*, 5392.
45. Cartier, L.; Okihara, T.; Ikada, Y.; Tsuji, H.; Puiggali, J.; Lotz, B. *Polymer* **2000**, *41*, 8909.
46. Garlotta, D. *J. Polym. Environ.* **2001**, *9*, 63.
47. Zhang, J. M.; Sato, H.; Tsuji, H.; Noda, I.; Ozaki, Y. *Macromolecules* **2005**, *38*, 1822.
48. Mooney, D. J.; Baldwin, D. F.; Suh, N. P.; Vacanti, J. P.; Langer, R. *Biomaterials* **1996**, *17*, 1417.
49. Domingos, M.; Intrauovo, F.; Gristina, A. G. R.; Ambrosio, L.; Bártolo, P. J.; Favia, P. *Acta Biomater* **2013**, *9*, 5997.
50. Ahmad, A. A.; Schubert, C.; Carvalho, C.; Thoman, Y.; Wittmer, A.; Metzger, M. *J. Biomed. Mater. Res. A* **2011**, *98A*, 303.
51. Georgiou, G.; Mathieu, L.; Pioletti, D. P.; Bourban, P. E.; Månson, J. A. E.; Knowles, J. C.; Nazhat, S. N. *J. Biomed. Mater. Res. B* **2006**, *10*, 322.
52. Seyednejad, H.; Gawlitta, D.; Kuiper, R. V.; Bruin, A.; Nostrum, C. F.; Vermonden, T.; Dhert, W. J. A.; Hennink, W. E. *Biomaterials* **2012**, *33*, 4309.
53. Karageorgiou, V.; Kaplan, D. *Biomaterials* **2005**, *26*, 5474.
54. Lebourg, M.; Antón, J. S.; Ribelles, J. L. G. *Eur. Polym. J.* **2008**, *44*, 2207.